Journal of Education for Pure Science
Vol.16, No. 02 (2026)
DOI: https://doi.org/ 10.32792/jeps.v16i2.786

Website: jceps.utq.edu.iq Email: jceps@eps.utq.edu.iq

Study of Cesium-Based Perovskite Solar Cells Incorporating Various Halides (I, Br, Cl)

Zahraa h. abbas[1], and Samir M. AbdulAlmohsin[*,1],

[1]Department of Physics College of Education, for Pure Disciplines University of Thi- Qar, Thi -Qar, 64001, Iraq

[*] Corresponding email: zahraa.hardan@utq.edu.iq

Received 08/09 /2025, Accepted 25 / 10 /2025, Published 01 / 06/2026

Abstract.

This work presents a comprehensive numerical investigation of all-inorganic tin-based halide perovskite solar cells employing three different absorber compositions: $CsSnCl_3$, $CsSnBr_3$, and $CsSnI_3$. The primary objective is to explain the effect of halide substitution on the structural, optical, and photovoltaic properties of the devices. Numerical simulations were performed by using SCAPS-1D, to systematically evaluate the influence of each halide on device production parameters. The proposed cell architecture uses MoS_2 as the electron transport layer owing to its high electron mobility and excellent structural stability, while WS_2 is employed as the hole transport layer to facilitate efficient hole extraction and suppress charge recombination. The comparative analysis reveals that halide composition plays a critical role in bandgap tuning and overall power conversion efficiency. Among the investigated absorbers, the $CsSnCl_3$-based device exhibited the best photovoltaic presentation, achieving a power conversion efficiency of 12.3%, a short-circuit current density of 16.9 mA/cm², and a fill factor of 18.9%. These findings highlight the potential of combining $CsSnCl_3$ with two-dimensional transition metal dichalcogenides (MoS_2/WS_2) as a promising strategy for developing stable, lead-free perovskite solar cells with enhanced performance.

Keywords: Perovskite Solar Cells, $CsSnX_3$, SCAPS-1D, MoS_2, WS_2, ETL, HTL.

1-Introduction

The rapid depletion of fossil fuel resources and their severe environmental consequences have made the development of renewable energy technologies a global priority. Among renewable energy sources, solar energy is considered one of the most promising and sustainable options for electricity generation, as photovoltaic devices enable the direct conversion of sunlight into electrical energy. In this context, perovskite solar cells (PSCs) have attracted significant attention owing to their outstanding optoelectronic properties, including high absorption coefficients, tunable band gaps, and the potential for low-cost fabrication.

Despite the remarkable progress achieved with lead-based perovskites, their long-term environmental and health concerns have motivated intensive research into lead-free alternatives. All-inorganic tin-based halide perovskites, represented by $CsSnX_3$ (X = Cl, Br, I), have emerged as promising candidates due to their suitable bandgaps, strong light absorption, and reduced toxicity compared to lead-containing counterparts. Nevertheless, the practical implementation of tin-based perovskites is hindered by several challenges, most notably the rapid oxidation of Sn^{2+}

to Sn^{4+} and the associated device instability. Consequently, the optimization of charge transport layers plays a critical role in improving carrier extraction, suppressing recombination, and enhancing overall device performance.
In recent years, two-dimensional transition metal dichalcogenides (TMDs) have gained increasing attention as efficient charge transport materials in photovoltaic applications. Materials such as MoS_2 and WS_2 exhibit favorable electronic properties, high carrier mobility, and excellent chemical stability, making them attractive candidates for electron and hole transport layers, respectively. Their atomically thin structure also facilitates improved interfacial contact with the perovskite absorber, which is essential for efficient charge separation and transport.

2-Novelty and Objectives of the Present Work

The novelty of this study lies in its systematic and comparative numerical analysis of all-inorganic, tin-based perovskite solar cells with different halide compositions—$CsSnCl_3$, $CsSnBr_3$, and $CsSnI_3$—evaluated within a single, unified device architecture. In contrast to most previous reports, which typically investigate only one halide absorber or employ conventional charge transport layers, this work introduces two-dimensional transition metal dichalcogenides, MoS_2 and WS_2, as the electron and hole transport layers, respectively. This design strategy allows for a comprehensive evaluation of the combined influence of halide substitution and 2D transport materials on bandgap tuning, charge transport behavior, and overall photovoltaic performance. The main objective of this study is to determine the optimal halide composition that delivers the highest power conversion efficiency while preserving the key benefits of lead-free and all-inorganic perovskite solar cells. [1].

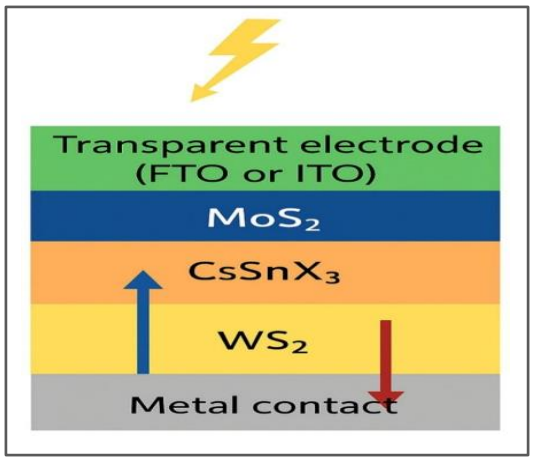

Fig1. Schematic of the $CsSnX_3$ Perovskite Astral Prison with MoS_2 and WS_2 Layers

Following the overview to tin-based perovskite solar cells and the importance of charge conveyance layers, it is essential to present the detailed layer construction of the wished-for solar lockup. The table below summarizes the materials cast-off in each layer, their respective functions, and typical thicknesses. This provides a clear understanding of the electron and hole pathways within the cell and helps analyze the impact of each layer on the device performance [2].

Table.1 Thickness and doping parameters used in the $Mos_2/CsSnX_3/WS_2$/Au solar cell simulation.

Layer	Thickness(nm)	Band gap(ev) Eg	Acceptor density ,N_A ($1/cm^3$)	Donor density ,N_D ($1/cm^3$)
Mos_2	30	1.4	------	10^{17}
$CsSnI_3$	400	1.5	------	-----
$CsSnCL_3$	400	2.2	------	----
$CsSnBr_3$	400	1.8	------	-----
WS_2	70	1.1	$10^{12} - 10^{16}$	-----

The MoS_2 layer, employed as the electron transport layer (ETL), exhibits a bandgap of approximately 1.4 eV and a relatively high donor concentration ($N_D \approx 10^{17}$ cm^{-3}), which promotes efficient electron extraction and enhances carrier mobility. In contrast, the WS_2 layer serves as the hole transport layer (HTL) and features a narrower bandgap of about 1.1 eV. Its capability to be doped across a wide acceptor concentration range ($N_A = 10^{12}$–10^{16} cm^{-3}) supports improved hole transport and collection.

The $CsSnX_3$ perovskite absorber layers exhibit a strong dependence of bandgap on halide composition, with approximate values of 1.5 eV for iodide, 1.8 eV for bromide, and 2.2 eV for chloride. This tunability enables effective control of the optical absorption spectrum. Since specific doping concentrations for these absorber layers are rarely reported in the literature, they are typically considered intrinsic or weakly doped in simulations to reduce bulk recombination and maintain favorable photovoltaic performance. [1]

3-Methodology

The studied all-inorganic tin-based perovskite solar cells consist of a layered architecture: MoS_2 as the electron transport layer (ETL), $CsSnX_3$ (X = Cl, Br, I) as the absorber, WS_2 as the hole transport layer (HTL), and metallic contacts. The ETL and HTL were selected for their high carrier mobility, chemical stability, and efficient charge extraction [2].

Numerical simulations were performed using SCAPS-1D, solving the coupled Poisson and continuity equations under AM1.5G illumination (1000 W/m^2) at 300 K. Material parameters, including bandgap, carrier mobility, permittivity, and defect density, were adopted from experimental and theoretical reports. Device performance parameterspower conversion efficiency (PCE), short-circuit current density (Jsc), open-circuit voltage (Voc), and fill factor (FF)were calculated for each halide composition to assess the effect of halide substitution and 2D transport layers on photovoltaic behavior.

4-Results and Discussion

The SCAPS-1D replication of all-inorganic cesium-based perovskite solar cells , employing MoS_2 as the electron transport sheet, WS_2 as the hole carriage sheet, and $CsSnX_3$ as the absorber, revealed that the $CsSnCl_3$-based device achieved the highest power conversion efficiency of 12.3% due to its optimal bandgap and favorable energy alignment [20]. This outcome is consistent with earlier studies highlighting the superior recital of $CsSnCl_3$ compared to $CsSnBr_3$ and $CsSnI_3$, primarily attributed to reduced recombination reat besides enhanced charge transport.

The analysis further showed that both sheet thickness and defect density play a crucial role in determining device performance. Right optimized thickness and lower defect density enhanced bright absorption and minimized recombination, while deviations in thickness or high defect density negatively affected efficiency, aligning with previous observations. Additionally, moderate doping of the transport sheets combined with a low-work-function back contact improved charge separation and further reduced recombination, thereby attractive overall efficiency.

In immediate, these findings accentuate that careful collection of halide composition, precise regulator over sheet thickness, defect management, and optimal drugging strategies are essential for achieving high-efficiency and stable all-inorganic perovskite solar cells. Among the materials studied, $CsSnCl_3$ consistently demonstrated superior performance within the MoS_2/WS_2 architecture, corroborating prior rumors [21].

Table (2) Upshot of Mos_2 Sheet Thickneness on Astral cell presentation limitations

Thickness (nm)Mos_2	$V_{OC(Volt)}$	J_{SC} (mA/cm²)	F.F(%)	$\pi_{(\%)}$
10	7.46	12.9	10.5	10.14
30	6.13	13.5	12.6	10.5
50	4.6	13.9	16.3	10.5
70	3.80	14.0	18.9	10.1

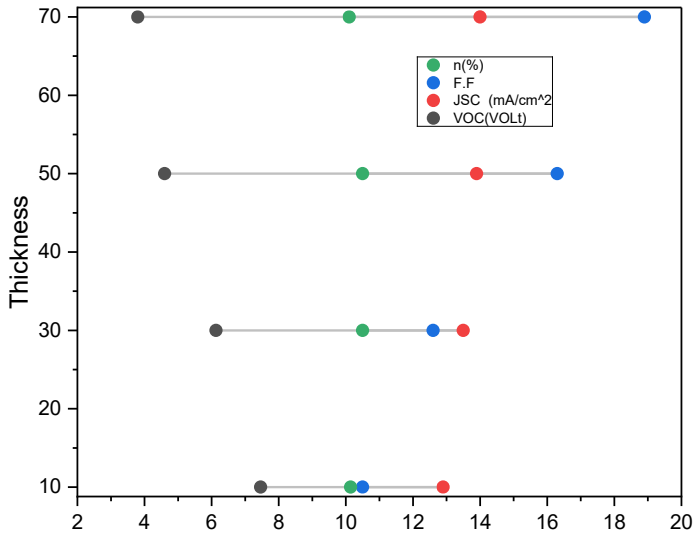

Fig (2): The disparity of Voc (volt), Jsc.(mA/cm^2), FF (%) and n (%) with thethickness Mos_2 of (nm)

The results indicate that the breadth of the MoS_2 sheet dramas a decisive protagonist in defining the photovolt presentation of the solar cells. When the MoS_2 thickness is limited to 10 nm, a relatively high open-route voltage (Voc) is achieved; however, the overall power conversion efficacy remains below its optimal value due to insufficient expectation transport. Increasing the thickness to anintermediate range of 30–50 nm leads to a more favorable trade-off between the brief-circuit recent density (Jsc) and the fill factor (FF), which collectively enhances charge extraction and reduces recombination Losses. As a result, the device attains its maximum efficiency, reaching approximately 10.5%. In contrast, further increasing the MoS_2 thicknessto 70 nm causes a pronounced reduction in Voc, likely due to increased series resistance and recombination effects, whi ch slightly degrades the overall efficiency. These findings confirm that moderate MoS_2 thicknesses provide the most balanced and efficient device performance. [3]

Table (3): Upshot of $CsSnX_3$ Layer Thicknes on Astral Lockup Demonstration Parameter

Thickness(nm) $CsSnX_3$	V_{OC}(Volt)	J_{SC} $(\frac{mA}{Cm^2})$	FF (%)	ɳ (%)
100	7.46	12.9	10.5	10.14
200	3.34	15.1	22.8	11.56
300	2.31	16.5	29.7	11.78
400	1.80	17.1	38.7	11.86
500	1.5	17.25	40.5	11.42

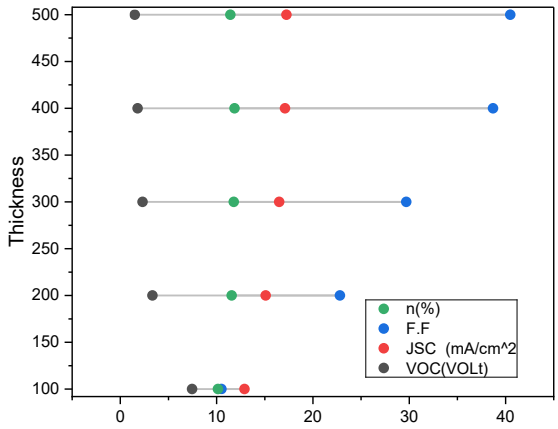

Fig (3): The disparity of Voc (volt), J_{sc} (mA/cm^2), FF (%) and η(%) with thethickness of $CsSnX_3$ (nm)

The numerical simul ation reveals that the thickness of the $CsSnX_3$ perovskite absorber sheet plays a central material in influential the photovoltaic presentation of the solar cells. When theabsorber thickness is limited to 100 nm, the device demonstrates an exceptionally high open- voltage; though, the short circuit current and fill factor remain relatively low, which restricts the total power conversion efficiency. Increasing the thickness to the range of 200–400 nm centrals to a noticeable enhancement in recent density and fill factor, mainly due to improved photon absorption and more effective charge carrier transport, while the open-circuit voltage shows a gradual decline. This opposing behavior among the photovoltaic parameters results in a continuous improvement in efficiency, reaching its maximum value at a thickness of approx imately 400 nm. Further increasing the absorber thickness to 500 nm causes a slight reduction in efficiency, despite higher current density and fill factor, which is likely associated with increased carrier recombination and voltage losses. Consequently, an absorber thickness near 400 nm represents an optimal condition that ensures a balanced interplay between carrier generation and recombination, thereby achieving the top device performance [5].

Table (4): Upshot of WS_2 Layer Thickness on Solar Cell Performance Parameters

Thickness (nm) WS_2	$V_{OC(VOLt)}$	J_{sc} $(\frac{mA}{cm^2})$	F.F (%)	ɳ (%)
10	7.46	12.9	10.5	10.14
30	6.5	13.5	11.9	10.3
40	6.29	13.7	12.37	10.7
60	5.4	14	13.3	11
70	5.8	14.4	13.3	11.18

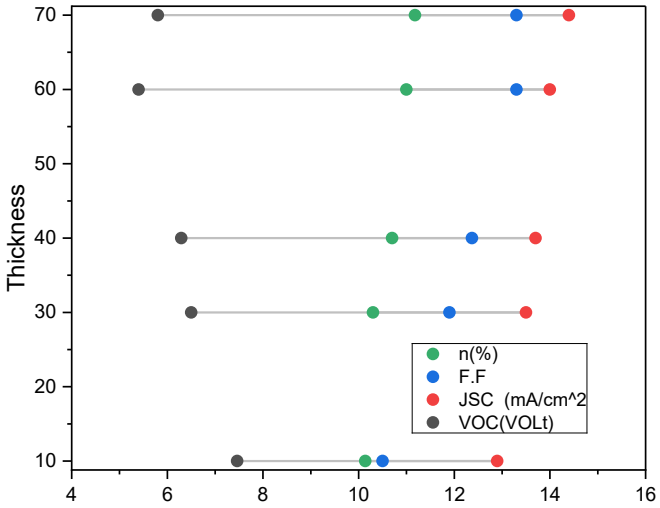

Fig (.4): The variation of Voc (volt), Jsc (mA/cm^2), FF (%) and η (%) with thethickn ess of WS_2

The analysis indicates that the thickness of the WS_2 layer has a notable influence on solar cells. As the thickness increase, V_{oc} declines, whereas both J_{sc} and FF improve, resulting in a gradual rise in efficiency. The best performance is observed at 70 nm, where the efficiency reaches about 11.18%. This suggests that employing a moderately thicker WS_2 layer (around 60–70 nm) provides the most favorable balance between charge generation and recombination, leading to optimal device operation [6].

The selected parameters and their corresponding efficiencies are summarized in the following table:

Table (5) Selected Optimal Thicknesses

Layer	Optimal Thickness (nm)	Achieved Efficiency (%)
Mos_2	30	10.5
WS_2	70	11.18
Perovskite	400	11.86

These thickness values were applied in a simulated solar cell structure in SCAPS, while other parameters were kept constant.

Table (6): Simulation Results

Layer Configuration	V_{oc} (volt)	J_{sc} $(\frac{mA}{Cm^2})$	F.F (%)	ɳ (%)
Mos_2 (30 nm) + WS_2 (70 nm) + Perov. (400 nm)	5.223	13.89	12.18	**11.04**

5- Result of Temperture on Solar Cell Performance

SCAPS-1D simulations were performed to assess the effect of temperature on an all-inorganic $CsSnX_3$ perovskite astral lockup, comprising WS_2 as the electron transport sheet and MoS_2 as the hole transport sheet. The results reveal that as temperature rises, the open-circuit voltage (Voc) decreases due to increased carrier recombination. Meanwhile, the short-circuit current density (Jsc) remains relatively unaffected, reflecting the stability of light absorption and charge generation processes. The fill factor (FF) exhibits a modest improvement with temperature, suggesting more efficient carrier extraction and reduced series resistance. Consequently, while higher temperatures negatively impact Voc, the overall power conversion efficiency shows only a slight reduction, importance the device's thermal resilience.

Table (7): Temperature Dependence of Solar Cell Performance

Temperature(k)	V_{oc} (volt)	J_{sc} $(\frac{mA}{Cm^2})$	F.F (%)	ɳ (%)
283	3.25	16.82	22.35	12.25
293	2.64	16.87	27.33	12.19
303	2.05	16.90	34.60	12.03
313	1.56	16.90	34.88	11.63
323	1.24	16.93	53.45	11.29
333	1.04	16.93	61.85	10.90
343	0.91	16.96	67.85	10.57

This table demonstrates the effect of fever on astral lockup productivity, which is reliable with previous findings reported in theliterature. (Improved from) [4]

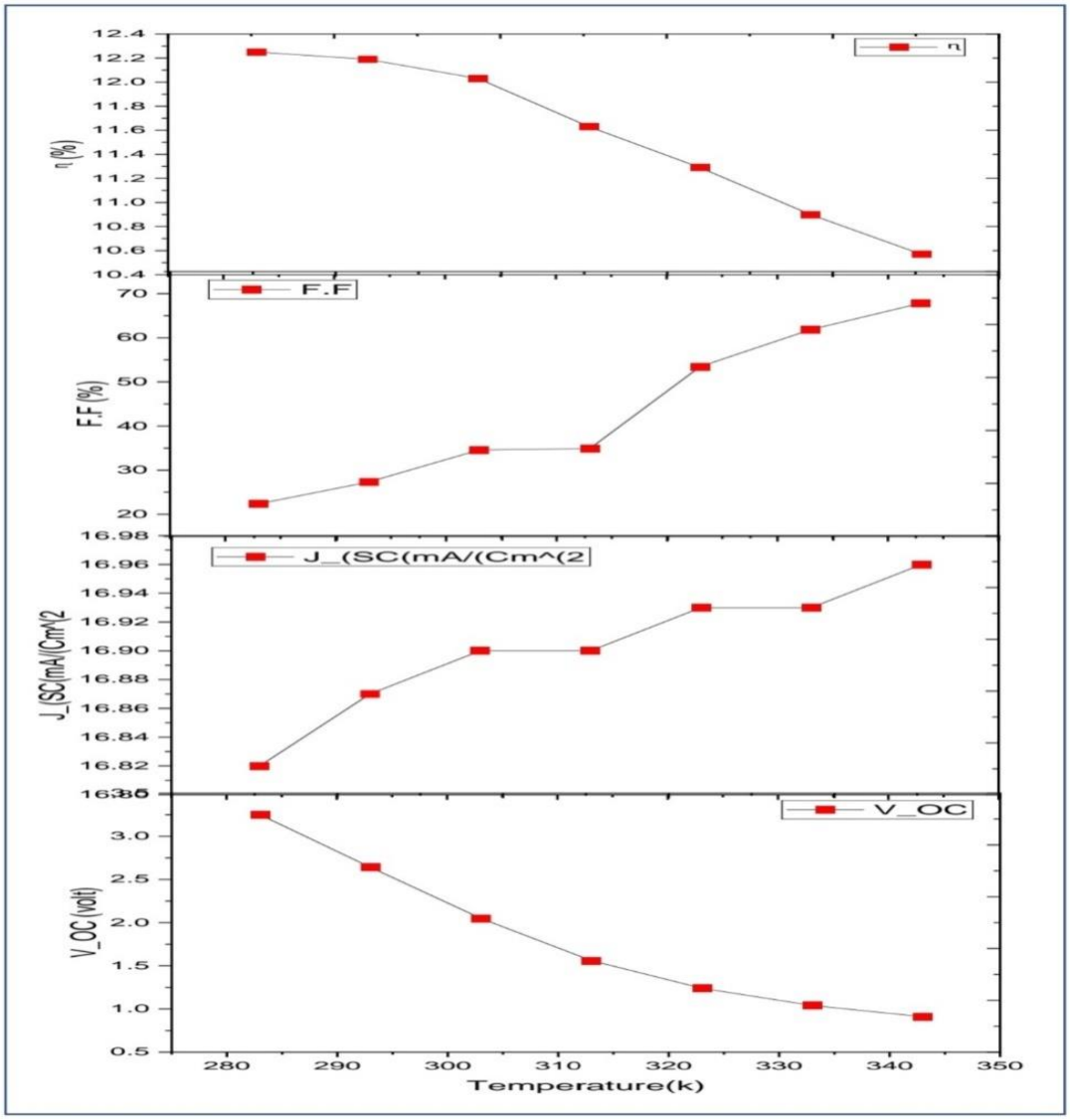

Fig (5): Outcome of Infection on V_{oc}, J_{sc}, Fill Factor, and Efficacy of the Astral Cell.

The results show that increasing temperature negatively moves the solar cell presentation by significantly reducing the not built up-circuit voltage (**V_{OC}**) and efficiency (η), owing to the rise in contrair overload recent. Meanwhile, the short-circuit current (**J_{sc}**) and fill factor (**FF**) slightly increase as a result of improved charge mobility and reduced internal resistance. However, the drop in voltage dominates, leading to an overall decline in efficiency

6-The Role of Band Gap in $CsSnX_3$ Layer Performance

The band gap dramas a main part in influential the efficacy of the $CsSnX_3$ perovskite layer by affecting its ability to absorb light and generate charge carriers. Proper control of the band gap enhances solar spectrum absorption and improves compatibility with other cell components, leading to better performance and stability

Approximate band gap values based on halogen sort

$CsSnCl_3 \approx 2.2eV$

$CsSnBr_3 \approx 1.8$ eV

$CsSnI_3 \approx 1.5$ eV

Table (8): Consequence of Energy Band Gap on the Performance of $CsSnCl_3$ Solar Cells

Energy band gap (ev) $CsSnCl_3$	V_{OC} (volt)	J_{SC} $(\frac{mA}{Cm^2})$	F.F (%)	ɳ (%)
2.2	3.8	16.9	18.9	12.3
2.4	3.8	16.9	18.9	12.3
3.8	3.8	16.9	18.9	12.3
3	3.8	16.9	18.9	12.3
3.2	3.8	16.9	18.9	12.3

Table (9): Result of Energy Band Gap on the Performance of $CsSnBr_3$ Solar Cells.

Energy band gap (ev) $CsSnBr_3$	V_{OC} (volt)	J_{SC} $(\frac{mA}{Cm^2})$	F.F (%)	ɳ (%)
1.5	0.6	17.4	66.9	7.8
1.6	0.7	17.4	63.0	10.4
1.7	0.9	17.5	39.6	10.6
1.8	1.7	17.5	40.1	12.0

Table (10): Result of Energy Band Gap on the Performance of $CsSnI_3$ Solar Cells

Energy band gap (ev) $CsSnI_3$	V_{OC} (volt)	J_{SC} $(\frac{mA}{Cm^2})$	F.F (%)	ɳ (%)
1.2	0.5	7.0	72.8	2.7
1.3	0.5	10.6	52.6	3.0
1.4	0.6	12.9	65.7	6.1
1.5	0.6	17.4	66.9	7.8

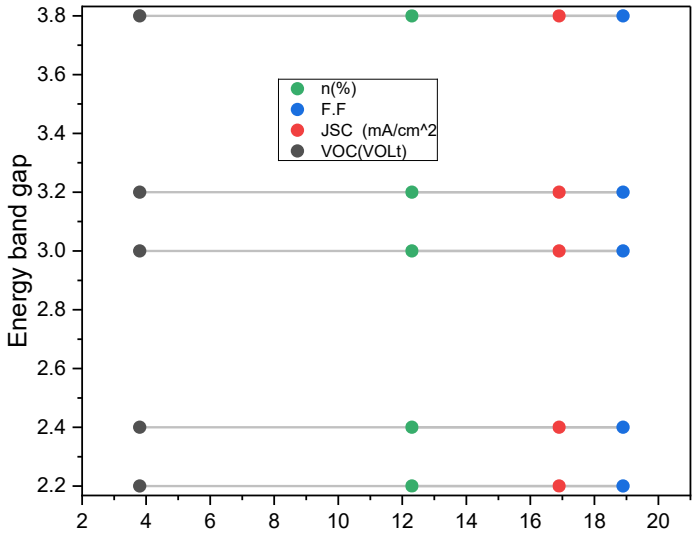

Fig (6): Characteristics of CsSncl₃ Solar Cells at Different Energy Band Gaps

Table (8) illustrates the outcome of the energy bandgap of $CsSnCl_3$ on the presentation of the simulated solar cells. Despite varying the band gap within the range (2.2 – 3.2 eV), all photovoltaic performance parameters remained unchanged, including the open-circute voltage (Voc =3.8V), short-circut current (Jsc=16.9) fill factor (F.F = 18.9%), and total power conversion efficiency (η = 12.3%)

This stability indicates that altering the band gap within this range does not significantly influence the photovoltaic properties of the material. It may also suggest that the applied simulation model does not exhibit sensitivity to band gap variations in thisdomain. Therefore, ($CsSnCl_3$) demonstrates remarkable performance stability regardless of band gap variations, which highlights its potential as a promising candidate for photovolt submissions requiring efficiency consistency [7,8]

Table (11): Influence of WS_2 Energy Band Gap on Photovoltaic Performance Parameters (V_{oc}, Jsc, F.F, η)

Energy-band gap WS_2	V_{OC} (volt)	J_{SC} $(\frac{mA}{Cm^2})$	F.F (%)	η (%)
1.1	1.6	16.9	40.6	11.6
1.2	1.6	16.9	40.6	11.6
1.3	1.6	16.9	40.6	11.6
1.4	1.6	16.9	40.6	11.6
1.5	1.6	16.9	40.6	11.6

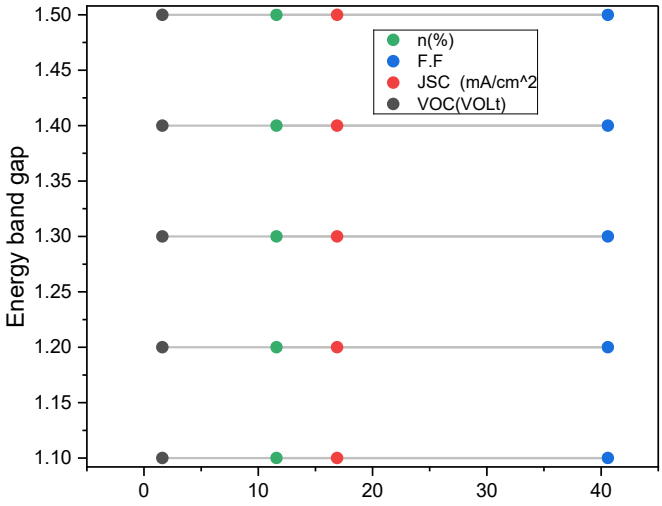

Fig(7): Variation of V_{oc}, Jsc, FF, and Efficiency with WS_2 Energy Band Gap

Table (11) demonstrates the result of varying the vigour bandgap of (WS_2) within the variety (1. 1 – 1.5 eV) on solar cell performance. The results clearly show that all photovoltaic parameters, including the open-course energy (V_{oc} = 1.6 V), short-circuit current J_{sc} = (16.9 mA/cm²), fill factor (FF = 40.6%), and efficiency (η = 11.6%), remained constant without any noticeable change [9].

This indicates that altering the energy band gap within this range does not influence the photovoltaic performance of WS_2, reflecting the stability of its optoelectronic properties. It may also suggest that the applied simulation model does not exhibit significant sensitivity to band gap variations in this domain.

Table (12): Effect of Mos_2 Energy Band Gap on Photovoltaic Parameters (V_{oc}, J_{sc}, F.F, η) of Solar Cell

Energy band gap Mos_2	V_{OC} (volt)	J_{sc} $(\frac{mA}{Cm^2})$	F.F (%)	η (%)
1.1	0.4	16.07	57.0	4.17
1.2	0.5	16.3	60.7	6.9
1.3	0.6	16.4	63.3	7.2
1.4	0.7	16.7	64.1	8.1

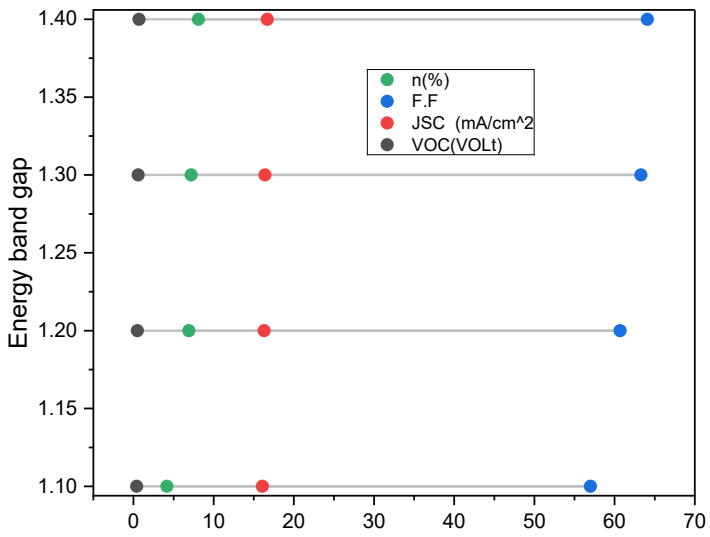

Fig (8): Effect of ene rgy gap on (V_{oc}, J_{sc}, F.F) and (efficiency).

The performance of solar cells was analyzed as a function of the MoS_2 bandgap using simulation data. Increasing the bandgap from 1.1 to 1.4 eV led to a rise in the open-circuit voltage (V_{oc}) since 0.4 to 0.7 V, indicating that a wider bandgap supports higher voltage generation. The short-circut current (J_{sc}) increased slightly from 16.07 to 16.7 mA/cm², showing minimal change in photocurrent with increasing bandgap

The fillfactor (FF) enhanced after 57% to 64.1%, due to better charge transport and reduced internal Losses. Consequently, the authority alteration efficiency enlarged since 4.17% to 8.1%, demonstrating a clear enhancement in overall solar cell performance with increasing MoS_2 bandgap [10].

These results indicate that adjusting the bandgap of the MoS_2 layer can directly influence the key performance parameters voltage, recent, fill factor, and efficiency and can be used as an effective approach to optimize solar cell performance.

Table (13): Consequence of Acceptor Compactness (N_A) on the Perfor mance of (WS_2) Layer.

Acceptor density, $N_A(1/cm^3)$	V_{OC} (volt)	J_{SC} $(\frac{mA}{Cm^2})$	F.F (%)	ɳ (%)
10^{12}	2.22	16.89	32.1	12.09
10^{13}	2.22	16.89	32.1	12.09
10^{14}	2.22	16.89	32.1	12.09
10^{15}	2.22	16.90	32.2	12.09
10^{16}	2.19	16.94	32.5	12.09

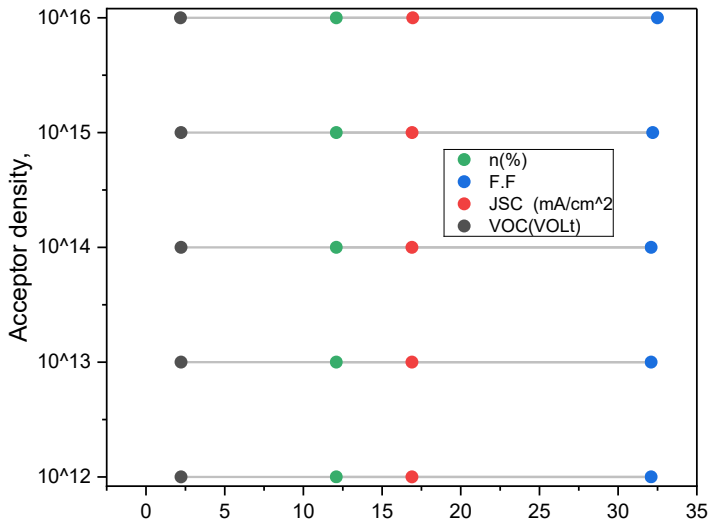

Figure (9): Variation of WS_2 Layer Parameters with Increasing Acceptor Density (N_A)

The results indicate that the power conversion efficiency (η) remains nearly constant at about 12.09% as the acceptor concentration (N_A) in the WS_2 layer increases from 10^{12} to 10^{16} cm^{-3}. This behavior suggests that the applied doping level is sufficient to improve the electrical conductivity of WS_2 without driving the material toward a fully conductive (metallic) regime. Moderate doping enhances hole transport, leading to slight increases in both the fill factor (FF) and the short-circuit current density (J_{SC}). However, these improvements are not substantial enough to produce a noticeable change in the overall device efficiency. Consequently, the results imply the existence of an optimal doping range that improves charge transport while preserving the semiconducting properties of WS_2, which are essential for efficient solar cell operation.

Table (14): Electrical Parameters of Mos_2Transport Layers with Donor Doping (N_D)

Donor density, N_D (1/ cm^3	V_{OC} (volt)	J_{SC} $(\frac{mA}{Cm^2})$	F.F (%)	ɳ (%)
10^{12}	2.22	16.89	23.18	12.09
10^{13}	2.22	16.89	23.18	12.09
10^{14}	2.22	16.89	23.18	12.09
10^{15}	2.22	16.90	30.1	12.1
10^{16}	2.22	16.94	32.23	12.14
10^{17}	2.22	17.15	31.7	12.49

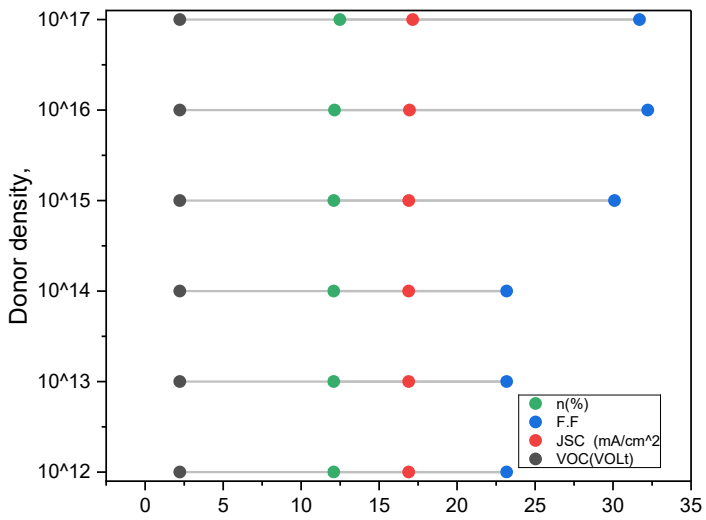

Figure (10): Electrical Parameters of Mos_2 Conveyance Layers with Donor Doping (N_D)

The results indicate that increasing the donor density (N_D) in the MoS_2 transport sheet from 10^{12} to$10^{17}cm^{-3}$ run to a perceptible upgrading in solar cells performance. Short circuit current (J_{sc}) increased after 16.89 to 17.15 mA/cm², the fill influence (FF) improved from 23.18% to 31.7%, and the efficacy (*n*) rose from 12.09% to 12.49%, while the open –circut voltage (V_{oc}) reach it to 2.22 V. This enhancement is attributed to better electrical conductivity of the MoS_2layer with higher N_D, which facilitated electron transport and reduced series resistance. However, the improvement remains moderate, suggesting that there is an optimal doping level that should not be exceeded to maintain the semiconducting properties of the layer [6]

7- Conclusion

The performance of an all-inorganic perovskite solar cell was numerically investigated using MoS_2 as the electron transport layer, WS_2 as the hole transport materials, and $CsSnCl_3$ as the absorber material. The improved maneuver achieved a power conversion efficiency of approximately 12.3%, benefiting from a suitable bandgap that enables efficient light absorption. The simulation results revealed that careful optimization of layer thicknesses, minimization of defect density, and the selection of a back-contact metal with a low work function play a crucial part in educating the full photovoltaic performance. Furthermore, an analysis of halide variation in CsSnX revealed that the selection of appropriate halides significantly influences device efficiency. In addition, moderate doping of the transport layers was found to augment care separation while suppressing recombination dead. These outcomes demonstrate the strong potential of the MoS_2/WS_2 architecture for the development of effective and steady all-inorganic perovskite astral lockups.

8-References

[1] **Ranjan. R., Anand.N., Tripathi. M. N., Srivastava, N., Sharma, A. K., Yoshimura, M., Chang, L., & Tiwari. R. N.** (2023). SCAPS-1D based examination of different pit transport layers for achieving high efficiency in eco-friendly CZTS astral lockups. Systematic Hearsays. 13(1), 18411. https:/doi.org/10.1038/s41598-023-44845-6.

[2] **Park, H.-J., Son, H., & Jeong, B.-S.** (2024). Efficiency optimization of lead-free $CsSnI_3$ perovskit astral lockups using SCAPS-1D simulation. Inorganics. 12(4), 123. https://doi.org/10.3390/inorganics12040123

[3] **Mohd Alias, A. N. S. N., et al.** (2022) Effect of aluminum incorporation in ZnO electron transport layers on perovskite astral lockup performance. Journal of Engineering and Technological Sciences, 54(4). https://doi.org/10.5614/j.eng.technol.sci.2022.54.4.9

[4] **Ferdous, W. M., et al.** (2023). Performance enhancement of MoS_2 heterojunction solar cells using Cu_2O as a hole conveyance veneer: A numerical reproduction study. Supplies Knowledges and Applications.14(9), 458–472. https:/doi.org/10.4236/msa.2023.149030.

[5] **Wang, X., et al.** (2022). Weathering performance of pressureless-sintered SiC exposed to molten NaCl–KCl–$MgCl_2$ salts at high temperature. Astral Vigor Materials besides Solar Lockups, 242, 111771. https://doi.org/10.1016/j.solmat.2022.111771

[6] **Becker, J. J., et al.** (2018). Monocrystalline MgCdTe solar cells with a 1.7 eV bandgap achieving 11.2% conversion efficacy. IEEE Periodical of Photovoltaics. 8(2), 581–586. https://doi.org/10.1109/JPHOTOV.2017.2769105

[7] **Oublal, E., Abdelkadir, A. A., & Sahal, M. (2022).** SCAPS-1D simulation of high-performance carbon nanotube-based solar cells incorporating CBTS as a spinal surface ground coating. Journal of Nanoparticle Research, 24(10), 202. https://doi.org/10.1007/s11051-022-05580-7

[8] Essaadia, O., et al. (2022). Numerical modeling of a two-terminal tandem solar cell employing narrow bandgap single-walled carbon nanotubes. Astral Liveliness, 246, 57–65. **https://doi.org/10.1016/j.solener.2022.09.036**

[9] **Paola, C.** (2014). Carbon nanotube/silicon mixture heterojunctions, for photovolt device applications. Fees in Nano Study, 2(1), 23. https://doi.org/10.12989/anr.2014.2.1.023**.**

[10] **Paola, C.** (2014). Carbon nanotube,silicon hybrid heterojunctions for photovolt devices, Advances in Nano Research, 2(1), 23. https://doi.org/10.12989/anr.2014.2.1.023

[11] **AbdulAmohsin, S. M., Cui, J. B., & Mohammed, M. Z. (2013).** Study on ZnO/P3HT:PCBM nanowire solar cells. In Proceedings of the 39th IEEE Photovoltaic Specialists Conference (PVSC). IEEE.https://doi.org/10.1109/PVSC.2013.6745026

[12] **AbdulAmohsin, S. M., Cui, J. B., & Mohammed, M. Z. (**2013). ZnO/P3HT:PCBM nanowire-grounded astral lockups: Design and performance analysis. 2013 IEEE 39th Photovolt Specialists Conference (PVSC). IEEE.

[13] **AbdulAmohsin, S. M., Cui, J. B., & Mohammed, M. Z.** (2013). Investigation of nanowire ZnO/P3HT:PCBM hybrid solar cells. In IEEE PVSC 2013. IEEE.DOI 10.11/PVSC.2013.6745026 (IEEE Xplore)

[14] **S. M. AbdulAlmohsin.** Hybrid Structure Organic / Inorganic Perovskites Solar Cells (Master's thesis). University of Thi-Qar. Retrieved April 15, 2025, (2021), from https://dspace.utq.edu.iq/handle/123456789/393 DOI 10.11/PVSC.2013.6745726

[15] **S. M. AbdulAlmohsin.** Study and Preparation of Solid State Dye Sensitized Solar Cell using D149 as a Dye, TiO_2 Nanoparticles as a Photo-anode and MWCNTs as a Counter Electrode (Master's thesis). *Iraqi Digital Repository. Retrieved April* 15, 2025, (2021), from https://iqdr.iq/search?view=d40dbb6ef271c1807d3594132b8453e5

[16] **Abdulsada, Z. R., & AbdulAlmohsin, S. M.** (2021). High-efficiency solar cells based on organic–inorganic perovskite materials. University of Thi-Qar Journal of Science, 8(2), 23–29. https://doi.org/10.32792/utq/utjsci.v8i2.808

[17] **Murtadha, J. E., et al.** (2024). Highest efficiency of perovskite-structure solar cells. International Journal of Thin Film Science and Technology, 13(1), 37–45.https://doi.org/10.18576/ijtfst/130105

[18] **Hussein, A. R., & AbdulAlmohsin, S. M.** (2024). Optimization of temperature, defect density, and thickness for achieving high-efficiency tin halide perovskite solar cells. Journal of Tutoring for Pure Science.14(2).https://doi.org/10.32792/jeps.v14i2.432

[19] **A. R. hussein, & S. M. AbdulAlmohsin,** O ptimization of Infection, Defects, and Thickness for Tall Efficacy of Tin Halide Perovskite. Journal of Instruction used for Clean Discipline. 14(2), (2024). https:/doi.org/10.32792/jeps.v14i2.432.

[20] **Yuan, S., Li, Z., Wang, Y., & Zhao, H.**, Theoretical Study and Analysis of $CsSnX_3$ (X = Cl, Br, I) All-Inorganic Perovskite Solar Cells with Different X-Site Elements, Molecules 29(11) (2024). DOI: 10.3390/molecules29112599 MDPI

[21] **SCAPS**-1D Simulation for Device Optimization to Improve Efficiency in Lead-Free CsSnI3 Perovskite Solar Cells, Inorganics 12(4) (2024). DOI:10.3390/inorganics12040123